Heliyon 10 (2024) e25293

Contents lists available at ScienceDirect

Heliyon

journal homepage: www.cell.com/heliyon

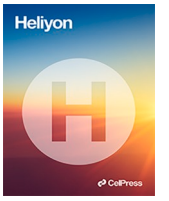

Research article

A general analytical solution for fluid flow and heat convection through arbitrary-shaped triangular ducts: A variational analysis

Amirhossein Hajiaghaei Tabalvandani [a], Mahmood Norouzi [a], Mohammad Hassan Kayhani [a], Amir Komeili Birjandi [a], Amin Emamian [a,b], Mirae Kim [c,**], Kyung Chun Kim [c,*]

[a] Faculty of Mechanical Engineering, Shahrood University of Technology, Shahrood, Iran
[b] Department of Mechanical Engineering, University of Bojnord, Bojnord, Iran
[c] School of Mechanical Engineering, Eco-friendly Smart Ship Parts Technology Innovation Center, Pusan National University, Busan, 46241, Republic of Korea

ARTICLE INFO

Keywords:
Arbitrary-shaped triangular ducts
Ritz method
Analytical solution
Heat transfer
Viscous dissipation

ABSTRACT

This paper presents an analytical solution for fluid flow and heat transfer inside arbitrarily-shaped triangular ducts for the first time. The former analytical solutions are limited to the special case of isosceles triangular ducts. The literature has no report about the analytical solution for the general case of arbitrarily-shaped triangular ducts. Due to the significant role of fluid flow through non-circular channels in industry and the large number of triangular shapes, a method for solving the heat transfer problem for all triangular shapes is needed. The heat transfer of a fluid flow through a channel with an arbitrary triangular cross-section for the case of constant heat flux at the walls is solved in this work for the first time, considering viscous dissipation. Here, the functionals of flow and heat transfer equations are derived, and the resulting Euler–Lagrange equations are solved using the Ritz method. The effect of the duct geometry on the velocity profile and friction coefficient is studied in detail. The effect of the Brinkman number on the temperature distribution and Nusselt number is investigated for both cooling and heating cases. The results reveal that the critical Brinkman Number distinguishes between the cooling and heating cases and represents the critical point at which the Nusselt number approaches infinity. The value of the Nusselt number decreases with the increase of the Brinkman number in both the wall cooling and heating modes. It is also found that the equilateral triangle exhibits the minimum friction coefficient and the maximum value of the Poiseuille number.

1. Introduction

The history of heat transfer of fluid flows through a duct dates back to ancient times. However, this field has attracted researchers in modern times due to its potential for designing high-performance equipment that can be used in various industrial and bioengineering applications. Recently, there has been considerable interest in applying non-circular and polygonal ducts in microfluidics and various fields of science and technology. These conduits find application in compact heat exchangers (CHE) and biological lab equipment such

* Corresponding author.
** Corresponding author.
E-mail addresses: futurekim@pusan.ac.kr (M. Kim), kckim@pusan.ac.kr (K.C. Kim).

https://doi.org/10.1016/j.heliyon.2024.e25293
Received 4 August 2023; Received in revised form 17 January 2024; Accepted 24 January 2024
Available online 30 January 2024

Nomenclature

A	Triangle's area
a	The unknown coefficients of Ritz
Br	Brinkman number
c	The specific heat capacity
C_f	The skin friction coefficient
D_h	The hydraulic diameter
f	Darcy friction factor
g	Gravity acceleration
h	Heat transfer coefficient
H	The triangle height
h_{loss}	The head loss
k	Conduction coefficient
L	Channel length
$\dot{m}$	Mass flow rate
Nu	Nusselt number
p	Pressure
Po	Poiseuille number
q'''	Heat source term
Re	Reynolds number
t	Time
T	Temperature
T_w	The wall temperature
T_m	The mean fluid flow temperature
u, v *and* w	Velocity in the x, y and z directions
$\boldsymbol{V}$	Velocity vector
w_0	The reference velocity
W	The average axial velocity
x, y and z	Cartesian coordinates
Ψ	Basis Ritz function
ρ	Density
μ	Viscosity
$\beta T \frac{DP}{Dt}$	The compressibility effect
$\dot{\gamma}$	The shear rate
φ	The section on viscosity losses in the energy equation
τ_w	The stress tensor
Γ	The triangle's perimeter

as DNA extraction, biosensors, blood sampling systems, and blood sugar monitoring. Many studies have been conducted to analyze the impact of various parameters on the design and manufacturing of heat exchangers. In these analyses, the impact of the configuration and geometry of cross-sections on the heat transfer is noteworthy.

Among the studies conducted on flow and heat transfer through non-circular ducts, Shah [1] investigated the fluid flow and heat transfer through forced convection under H1, H2, and constant wall temperature boundary conditions inside ducts with different cross-section shapes. He utilized the least-squares fitting method and showed that the highest Nusselt and Poiseuille numbers among the isosceles triangles are associated with an equilateral triangle. He also disclosed that the Nusselt number reaches its maximum value under H1 and H2 cases, respectively.

The literature also has approximate solutions for forced convection heat transfer and fluid flow within triangular ducts [2–4]. An analytical study was conducted by Aparecido and Cotta [5] on the developed laminar flow through right Triangular ducts subjected to constant wall temperature conditions for Newtonian fluids. Etemad et al. [6] conducted a 3D Galerkin finite-element thermal analysis for the case of non-Newtonian fluid flow in equilateral triangular channels. It is demonstrated that changing the shear-thinning intensity of the fluid influences the variations of the local Nusselt numbers.

Chen et al. [7] studied numerically the fluid flow and heat transfer within triangular ducts characterized by varying vertex angles. Their response demonstrated a good agreement with previous data. Chaves et al. [8] also investigated generalized Newtonian fluid flow and heat transfer through triangular closed channels. They applied a mixed analytical-numerical method using the generalized integral transformation. The study considered constant wall temperature for right and isosceles triangular ducts.

Hooman and Haji-Sheikh [9] studied the forced convection of the fully developed flow through a saturated porous channel with a rectangular cross-section by considering the viscous dissipation under uniform heat flux and constant wall temperature boundary conditions. The findings indicated that an increase in the impact of viscous dissipation leads to a reduction in the Nusselt number.

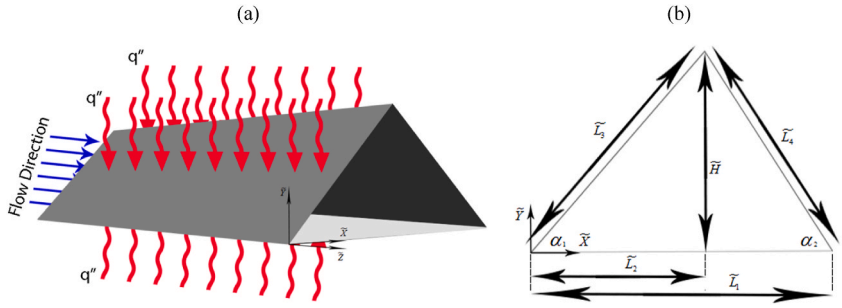

Fig. 1. (a) The geometry of the channel and (b) the geometrical parameters of the cross-section.

Zhang [10] also studied forced convection heat transfer and fully-developed laminar flow through ducts with isosceles triangular cross-sections used in compact plate-fin heat exchangers involving a wide range of isosceles triangles with vertex angles of 30–120 and a fin conductance parameter ranging from 0 to infinity. Consequently, Nusselt numbers are derived for different vertex angles and fin conductance parameters. These values can be applied for thermal analysis of compact heat exchangers.

Ray and Misra [11] investigated the head loss and thermal characteristics of fully-developed flow within channels having square and equilateral triangular cross-sections with rounded corners for H1 and H2 cases. The non-dimensional radius of the corners' curve for square ducts was considered from 0 to the maximum possible value of 1, while for the equilateral triangular ducts, it was in the range of 0–1.732. Among the other studies, Wang [12,13] studied analytically the fully developed slip flow under H1 boundary conditions through triangular and rectangular ducts and the oscillatory and transient fluid flow in equilateral triangular channels. Furthermore, Wang [14–16] presented the Ritz solutions for the slip flow under constant heat flux through isosceles triangular ducts, the fully developed Dean flow, and the oscillatory flow in elliptic and isosceles triangular channels. Karabulut et al. [17] reported a thermal analysis for fully developed flow in the case of constant wall temperature. They also mentioned its application in parabolic and isosceles triangular ducts. Hung [18] studied the heat convection of fully developed nanofluid flows in microchannels analytically. He investigated the impacts of the Brinkman number on temperature distribution.

Hung and Tso [19] investigated forced convection heat transfer in a fully developed flow within a homogeneous porous medium. The study examined the influence of viscous dissipation on heat transfer, and the Nusselt number was determined as a function of Darcy and Brinkman numbers. Aydin [20] investigated the effect of viscous dissipation on Newtonian flow and heat transfer inside a pipe with uniform heat flux and wall temperature. Aydin and Avci [21] analytically investigated laminar Couette-Poiseuille flow and heat transfer for Newtonian fluids with constant properties. Their study also took into account the influence of viscous dissipation. Norouzi et al. [22] recently provided an exact thermal analysis for flow in equilateral triangle closed channels. The study extensively examined the influence of the Brinkman number. The findings emphasize the significance of viscous dissipation in the flow of highly viscous fluids in microchannels. Using computational fluid dynamics, Kose et al. [23] numerically investigated laminar fluid flow and heat convection in microchannel heat sinks in three distinct shapes. They proposed that a triangle with an apex angle of 50° is the optimal geometric parameter for triangular microchannels. The 3D airflow on the performance of microchannel heat sinks with five different geometries was investigated by Moradikazerounia et al. [24]. The findings indicated that the triangular shape offers the highest Nusselt number for cooling case of a given microchannel heat sink among the other shape of cross-sections.

According to the literature, most studies on fluid flow and heat convection inside triangular channels are limited to numerical analysis that deals with specific triangle geometry in which the effect of the Brinkman number has not been considered. On the contrary, the present study proposes an analytical solution for heat convection in arbitrary triangular cross-sections by considering viscous dissipation for the first time. The solution is carried out via the Ritz method, categorized as a variational method to solve linear and nonlinear partial differential equations. Formulating a general analytical solution for flow and heat convection in a complex geometry poses considerable challenges. This difficulty forms the crux of innovation in the current research. We also studied how geometry and viscous dissipation influence the axial velocity and temperature and evaluated the head loss and Nusselt number via this analytical solution. The schematic geometry of the problem is depicted in Fig. 1.

2. Mathematical formulation

2.1. Governing equation

The governing equations of the current study are as follows [25]:

$$D\rho/_{Dt} + \rho\nabla\cdot\widetilde{\boldsymbol{V}} = 0 \tag{1}$$

$$\rho D\widetilde{\boldsymbol{V}} \,/\, Dt = -\nabla\widetilde{p} + \rho\widetilde{\mathbf{g}} + \mu\nabla^2\widetilde{\boldsymbol{V}} \tag{2}$$

$$\rho c D\widetilde{T} \,/\, Dt = \nabla\cdot(k\nabla\widetilde{T}) + q''' + \beta\widetilde{T}D\widetilde{p} \,/\, Dt + \mu\varphi \tag{3a}$$

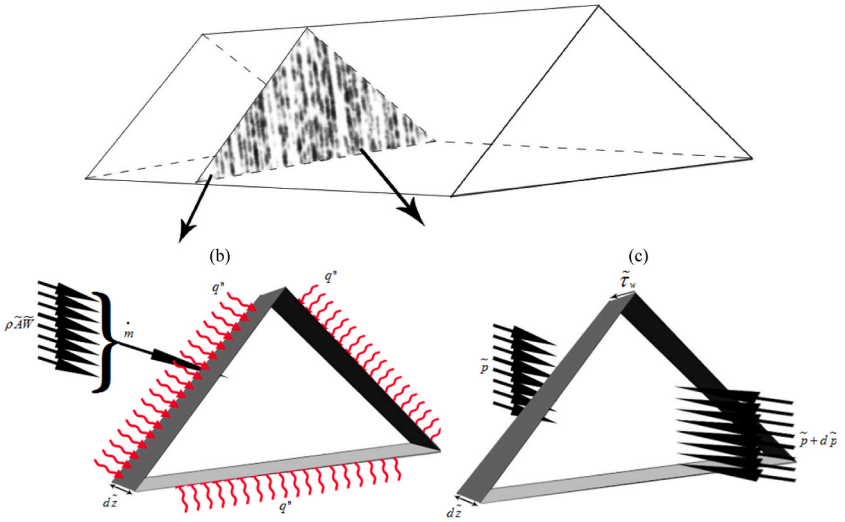

Fig. 2. (a) A duct with a triangular cross-section, (b) the thermal energy equilibrium within a differential control volume, (c) the equilibrium of applied forces within a differential control volume.

Eq. (1) is the continuity equation, which states that the rate of the mass entering a system is equal to the sum of the rate of the mass leaving the system and the accumulation of the mass in the system. Eq. (2) is the momentum equation that represents the equilibrium of the transient force on the fluid in a part of the channel cross-section. The left side is mass times acceleration where ρ is density, t is time, and $\widetilde{V}$ is velocity. The right side shows the forces applied to the fluid, including pressure gradient, gravitational force, and frictional force where $\widetilde{p}$ is pressure, $\widetilde{\mathbf{g}}$ is gravity acceleration, μ is viscosity. The energy equation (Eq. (3)) is an expression of energy conservation. On the left side, it represents the variation of energy inside a fluid element where c is specific heat capacity and $\widetilde{T}$ is temperature. The right side represents the effects of conduction, heat source and sink, the work of compressibility, and the viscous dissipation (φ). Moreover, $\widetilde{u}$, $\widetilde{v}$ and $\widetilde{w}$ are velocity in the $\widetilde{x}$, $\widetilde{y}$ and $\widetilde{z}$ directions in Cartesian coordinates, respectively. For the problem being considered here, the flow is steady and fully developed with a constant thermal conductivity coefficient, and the heat source/sink term is neglected.

The non-dimensional parameters related to the governing equations are defined as follows [22]:

$$x=\widetilde{x}/D_h \quad y=\widetilde{y}/D_h \quad Br=\mu\widetilde{W}^2/q''D_h \quad \Gamma=\widetilde{\Gamma}/D_h \quad W=\widetilde{W}/w_0$$

$$\dot{\gamma}=\dot{\widetilde{\gamma}}D_h\Big/w_0 \quad z=\widetilde{z}\Big/D_h \quad T=\widetilde{T}-\widetilde{T}_w\Big/q''D_h/k \quad A=\widetilde{A}\Big/D_h^2 \quad \tau_w=D_h\widetilde{\tau}_w\Big/\mu w_0 \tag{4}$$

where $\widetilde{A}$ and $\widetilde{\Gamma}$ are the triangle's area and perimeter, respectively, $\widetilde{w}$ is the axial velocity, $\dot{\gamma}$ is the shear rate, Br is Brinkman number, $\widetilde{\tau}_w$ is the wall shear stress, D_h is the hydraulic diameter, $\widetilde{W}$ is the mean velocity, $\widetilde{T}_m$ is the mean fluid flow temperature, and w_0 is the reference velocity. In addition, the hydraulic diameter, the mean temperature, the mean velocity, and the reference velocity, which correspond to the parameters of the triangular geometry, are described in Eqs. ((5) to (8)) [22]:

$$D_h=4\widetilde{A}/\Gamma \tag{5}$$

$$\widetilde{T}_m=(1/\widetilde{W}\widetilde{A})\int\widetilde{w}\widetilde{T}d\widetilde{A} \tag{6}$$

$$\widetilde{W}=(1/\widetilde{A})\int\widetilde{w}d\widetilde{A} \tag{7}$$

$$w_0=-(D_h^2/16\mu)d\widetilde{p}/d\widetilde{z} \tag{8}$$

The dimensionless form of the momentum equation is presented in Eq. (9):

$$\left(\partial^2w/\partial x^2\right)+\left(\partial^2w/\partial y^2\right)=-16 \tag{9}$$

Fig. 2 depicts a differential control volume of the flow field.

Considering the differential control volume (Fig. 2a(and applying the equilibrium of energy within a differential control volume

(Fig. 2b), the mean temperature variation in the axial direction of the channel is expressed as follows:

$$q''\widetilde{\Gamma}d\widetilde{z}+\int\varphi d\widetilde{A}d\widetilde{z}=\dot{m}(h_{z+dz}-h_z) \tag{10a}$$

$$q''\widetilde{\Gamma}d\widetilde{z}+\int\mu\left((\partial\widetilde{w}/\partial\widetilde{x})^2+(\partial\widetilde{w}/\partial\widetilde{y})^2\right)d\widetilde{A}d\widetilde{z}=\rho\widetilde{A}\widetilde{W}cd\widetilde{T}_m \tag{10b}$$

$$4q''\Big/\rho\widetilde{W}cD_h+\mu\int\left((\partial\widetilde{w}/\partial\widetilde{x})^2+(\partial\widetilde{w}/\partial\widetilde{y})^2\right)d\widetilde{A}\Big/\rho\widetilde{A}\widetilde{W}c=d\widetilde{T}_m\Big/d\widetilde{z} \tag{10c}$$

The energy balance on the differential control volume is presented in Eqs. (10a) and (10b). Given that the flow is thermally fully developed $\left(\partial(\widetilde{T}-\widetilde{T}_w/\widetilde{T}_m-\widetilde{T}_w)_{/\partial\widetilde{z}}=0\right)$ with constant heat flux at walls $(q''=h(\widetilde{T}_w-\widetilde{T}_m))$ by considering Eq. (10c), we have:

$$d\widetilde{T}_m\Big/d\widetilde{z}=d\widetilde{T}_w\Big/d\widetilde{z}=\partial\widetilde{T}\Big/\partial\widetilde{z}=q''\widetilde{\Gamma}\Big/\rho\widetilde{A}\widetilde{W}c+\mu\int\left((\partial\widetilde{w}/\partial\widetilde{x})^2+(\partial\widetilde{w}/\partial\widetilde{y})^2\right)d\widetilde{A}\Big/\rho\widetilde{A}\widetilde{W}c \tag{11}$$

Substituting Eq. (11) into Eq. (3), the dimensionless heat transfer equation will be attained as follows:

$$\left(\partial^2T/\partial x^2+\partial^2T/\partial y^2\right)=(4w/W)+\left(Br/W^2\right)\left((w/WA)\int\left((\partial w/\partial x)^2+(\partial w/\partial y)^2\right)dA-\left((\partial w/\partial x)^2+(\partial w/\partial y)^2\right)\right) \tag{12}$$

In the above, the Brinkman number, Br, signifies the impact of viscose dissipation. If Br is set to zero, dissipation is ignored in the energy equation.

2.2. Friction coefficient and Nusselt number

The primary consequence of viscosity in any internal fluid flow is pressure drop. Remember that the viscosity causes a force of friction at walls. The pressure drop equation based on the shear stress at the wall can be obtained by applying the balance of forces over a differential element of the channel (as shown in Fig. 2c). As the acceleration is zero for the steady flow in the fully developed region, we have:

$$-d\widetilde{p}\Big/d\widetilde{z}=(1/\widetilde{A})\int\widetilde{\tau}_w d\widetilde{\Gamma} \tag{13}$$

Eq. (13) is the balance of forces acting on a differential element of the channel. Since the flow is fully developed, the pressure gradient is a negative constant ($-\Delta\widetilde{p}=\rho\widetilde{g}\widetilde{h}_{loss}$) where $\widetilde{h}_{loss}$ denotes the head loss and is defined by the Darcy– Weisbach equation as below:

$$\widetilde{h}_{loss}=f\widetilde{L}\widetilde{W}^2/D_h2\widetilde{g} \tag{14}$$

In Eq. (14), f is the Darcy friction factor. By substituting Eq. (14) into the pressure equation, also considering $\widetilde{\tau}_w=\mu\widetilde{\dot{\gamma}}$ and $\widetilde{\dot{\gamma}}=\sqrt{(\partial\widetilde{w}/\partial\widetilde{x})^2+(\partial\widetilde{w}/\partial\widetilde{y})^2}$, the dimensionless friction relation will be obtained as:

$$f.Re=Po=2\int\dot{\gamma}d\Gamma\Big/\int wdA \tag{15}$$

In Eq. (15), Po represents the Poiseuille number, and it is equal to the multiplication of f and the Reynolds number [26]. The skin friction coefficient is written in Eq. (16) for laminar flow as follows [25]:

$$C_f=\frac{\mu\widetilde{\dot{\gamma}}}{\rho\widetilde{W}^2/2} \tag{16}$$

$$C_f.Re=2\dot{\gamma}/W \tag{17}$$

Eq. (17) is the non-dimensional form of the skin friction coefficient equation. The convection coefficient is calculated as follows:

$$h=q''/(\widetilde{T}_w-\widetilde{T}_m) \tag{18}$$

By substituting the dimensionless form of Eq. (18) into the Nusselt equation $(Nu=hD_h/k)$, the Nusselt number can be represented as Eq. (19):

$$Nu = -\int wdA \Big/ \int wTdA \tag{19}$$

3. Analytical solution

The current study applied the Ritz method [27] to solve flow and heat transfer in triangular ducts. The Ritz method is based on the calculus of variations. Here, it was adopted to solve the flow and heat transfer equations for triangular ducts. Consider the function $F(x, y, T, T_x, T_y)$, where x and y are independent variables, and T is the unknown parameter of interest. Tx and Ty also denote the partial T derivative to x and y. In the Ritz method, the problem is formulated in terms of an integral of a functional and is defined in Eq. (20):

$$I = \iint_R F\left(x, y, T, T_x, T_y\right) dxdy \tag{20}$$

The necessary condition for T to have an extremum for a given functional I is that function F satisfies the following Euler–Lagrange equation [28]:

$$\partial F / \partial T - \partial(\partial F / \partial T_x) / \partial x - \partial\left(\partial F / \partial T_y\right) / \partial y = 0 \tag{21}$$

A necessary condition for functional I to have an extremum is that δI must be zero. To prove this point, the change in function $F(x, y, T, T_x, T_y)$ according to the variation of T for fixed x and y (the value of T is considered constant at boundaries) is written as follows:

$$\delta F = F\left(x, y, T + \delta T, T_x + \delta T_x, T_y + \delta T_y\right) - F\left(x, y, T, T_x, T_y\right) \tag{22}$$

After applying the two-dimensional Taylor series expansion for Eq. (22) and considering $\delta I = 0$, Eq. (23) results:

$$\delta I = \iint_R \left((\partial F / \partial T)\delta T + (\partial F / \partial T_x)\delta T_x + \left(\partial F / \partial T_y\right)\delta T_y\right) dxdy = 0 \tag{23}$$

Using the simplification of the second and third terms of Eq. (23) by integration by part, the above equation is reduced to:

$$\delta I = \iint_R \left\{(\partial F / \partial T) - \partial\left(\partial F / \partial T_x\right) \Big/ \partial x - \partial\left(\partial F / \partial T_y\right) \Big/ \partial y\right\} \delta T dxdy = 0 \tag{24}$$

It can also be written in the form of Euler equation (Eq. (21)), which is the necessary condition for I to be stationary. This result can be used for solving the problem by the Ritz method, which is based on the selection of a convergent sequence of functions as follows:

$$w(x, y) = \sum_{i=1}^{N} a_i \psi_i(x, y) \tag{25}$$

where $\psi_i(x, y)$ satisfies the boundary conditions for all values of i. In Eq. (25), w is the unknown of the problem (velocity), a_i are the unknown coefficients of Ritz, and $\psi_i(x, y)$ are the basis functions of the Ritz method. N equations and N unknowns appear by selecting an appropriate term number of series (N) and placing it in Eq. (24). After solving this system of equations, the unknown coefficients a_i are obtained. Then, the problem can be solved by placing these coefficients in the series.

To calculate $\psi_i(x, y)$ in the present study, the equation of the lines representing the sides of a triangle was multiplied. Therefore, the value of $\psi_i(x, y)$ on the boundaries is always zero. Eq. (26) indicates $\widetilde{\psi}$ whereas Eq. (27) shows its dimensionless form. The series used to solve the problem is also given in Eq. (28). In this study, ψ is the "basis Ritz function" which the Ritz functions were written based on it:

$$\widetilde{\psi} = \widetilde{y}(\widetilde{y} - (\widetilde{H} / \widetilde{L}_2)\widetilde{x})(\widetilde{y} - (\widetilde{H} / (\widetilde{L}_2 - \widetilde{L}_1))\widetilde{x} - (\widetilde{L}_1 / (\widetilde{L}_1 - \widetilde{L}_2))\widetilde{H}) \tag{26}$$

$$\psi = y(y - (H / L_2)x)\left(y - (H / (L_2 - L_1))x - \left(\left(L_1 + \sqrt{H^2 + L_2^2} + \sqrt{H^2 + (L_1 - L_2)^2}\right) \Big/ 2(L_1 - L_2)\right)\right) \tag{27}$$

$$\psi_1(x, y) = x^0 y^0 \psi(x, y)$$

$$\psi_2(x, y) = x\psi(x, y)$$

$$\psi_3(x, y) = y\psi(x, y)$$

$$\psi_4(x, y) = xy\psi(x, y)$$

$$\psi_5(x, y) = x^2\psi(x, y)$$

$$\psi_6(x, y) = y^2\psi(x, y)$$

$$\vdots \psi_{28}(x, y) = y^6\psi(x, y) \tag{28}$$

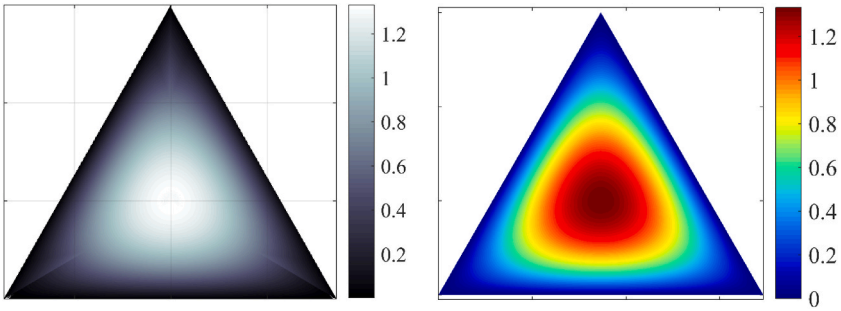

Fig. 3. Velocity distribution contours for equilateral triangle (a) Ref. [29] and (b) current study.

Table 1
Poiseuille number for isosceles and right triangles.

α	Poiseuille number for Isosceles triangle				Error (%)			Poiseuille number for right triangle		Error (%)
	Ref. [1]	Ref. [3]	Ref. [30]	Present study	ϵ_1	ϵ_2	ϵ_3	Ref. [3]	Present study	ϵ_4
10	49.9	50	–	49.8	0.2	0.4	–	50	49.8	0.4
20	51.3	51.2	51.6	51.2	0.195	0	0.775	51.2	51.2	0
30	52.3	52.2	–	52.2	0.191	0	–	52	52.1	0.192
40	52.9	52.8	52.9	52.9	0	0.189	0	52.5	52.5	0
50	53.2	53.2	–	53.2	0	0	–	52.5	52.5	0
60	53.3	53.3	53.3	53.3	0	0	0	52	52.1	0.192
70	53.2	53.2	–	53.2	0	0	–	51.2	51.2	0
80	53	52.9	52.9	53	0	0.189	0.189	50	49.8	0.4
90	52.6	52.7	–	52.6	0	0.19	–	–	–	–
100	–	52	52	52	–	0	0	–	–	–
120	51	51	51.1	51	0	0	0.196	–	–	–
140	–	49.5	49.5	49.7	–	0.404	0.404	–	–	–
150	48.9	48.8	–	49.1	0.409	0.615	–	–	–	–
160	–	48.3	48.3	48.6	–	0.621	0.621	–	–	–

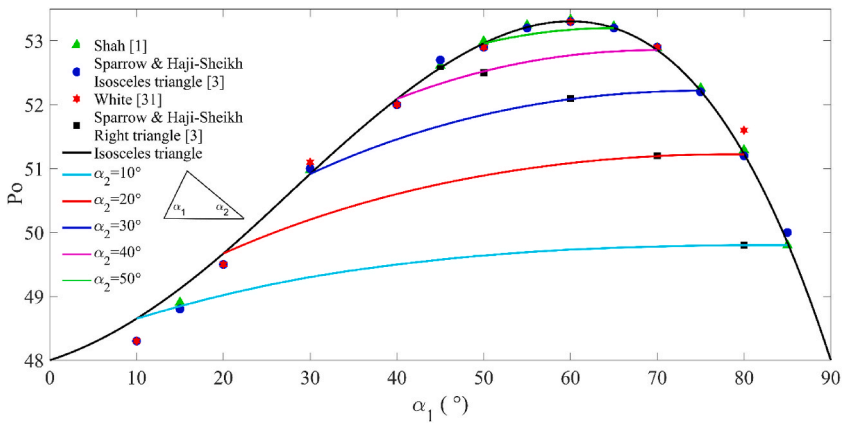

Fig. 4. Poiseuille number for arbitrary triangles.

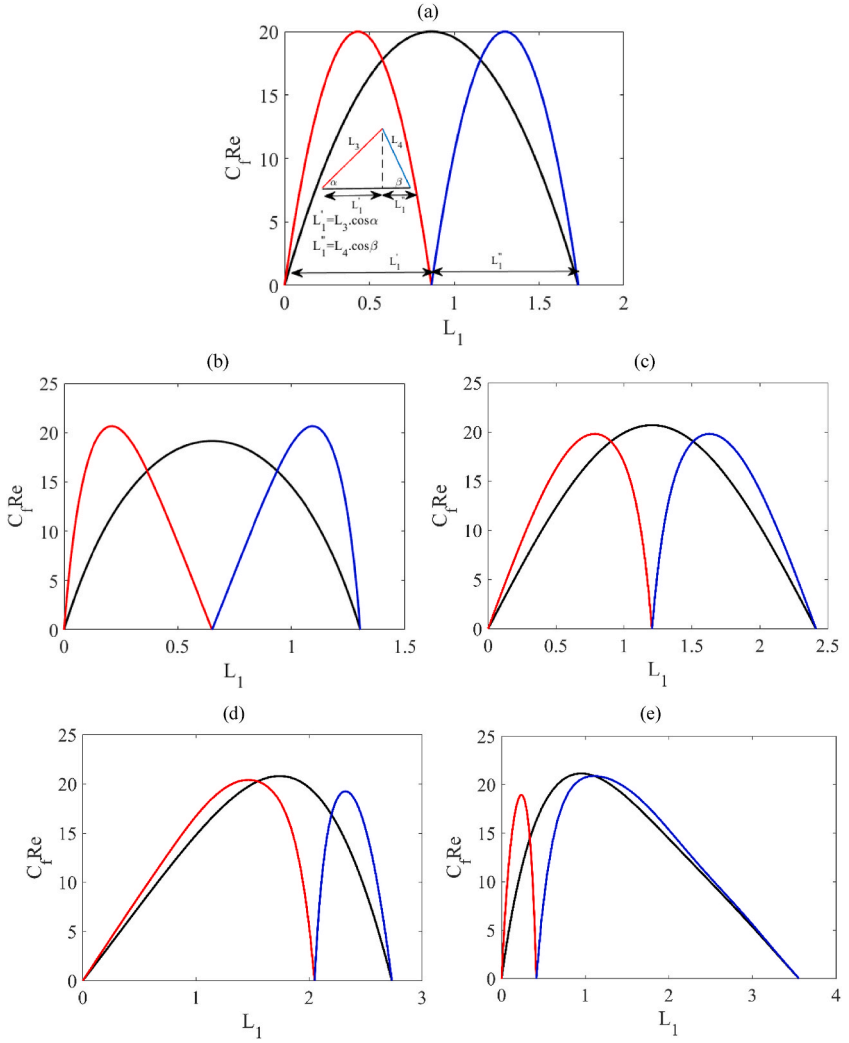

Fig. 5. The skin friction coefficient for (a) equilateral triangle (isosceles triangle $\alpha_1 = \alpha_2 = 60$), (b) isosceles triangle $\alpha_1 = \alpha_2 = 75$, (c) isosceles triangle $\alpha_1 = \alpha_2 = 45$, (d) right triangle $\alpha_1 = 30$ and $\alpha_2 = 60$, and (e) right triangle $\alpha_1 = 70$ and $\alpha_2 = 20$.

$$w(x,y) = \sum_{i=1}^{N} a_i \psi_i(x,y) = \psi(x,y)\left(a_1 + a_2 x + a_3 y + \ldots a_{28} y^6\right) \tag{29}$$

Eq. (29) represents the fluid velocity in the axial direction, and its value at the boundaries equals zero. According to the mentioned dimensionless parameter for temperature, the dimensionless temperature on the walls is equal to zero. Therefore, the same velocity series can be used for temperature:

$$T(x,y) = \sum_{i=1}^{N} a_i \psi_i(x,y) = \psi(x,y)\left(a_1 + a_2 x + a_3 y + \ldots a_{28} y^6\right) \tag{30}$$

Taking the momentum equation as the Euler equation of the variational formulation (and the energy equation to find the temperature), we have from Eq. (24)

$$\delta I = \iint_R \left\{\partial^2 w / \partial x^2 + \partial^2 w / \partial y^2 + 16\right\} \delta w dx dy = 0 \tag{31}$$

for velocity and

Table 2
Nusselt number for isosceles and right triangles.

α	Nusselt number for Isosceles triangle 			Error (%)		Nusselt number for right triangle 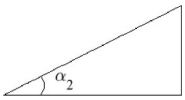		Error (%)
	Ref. [1]	Ref. [3]	Present study	ϵ_1	ϵ_2	Ref. [3]	Present study	ϵ_3
10	2.45	2.46	2.46	0.408	0	2.44	2.45	0.41
20	2.72	2.72	2.73	0.368	0.368	2.72	2.72	0
30	2.91	2.91	2.91	0	0	2.88	2.89	0.347
40	3.03	3.03	3.03	0	0	2.97	2.97	0
50	3.09	3.1	3.09	0	0.323	2.97	2.97	0
60	3.11	3.11	3.11	0	0	2.88	2.89	0.347
70	3.1	3.1	3.1	0	0	2.72	2.72	0
80	3.05	3.06	3.05	0	0.327	2.44	2.45	0.41
90	2.98	2.99	2.98	0	0.334	–	–	
100	–	2.9	2.9	–	0	–	–	
120	2.68	2.68	2.68	0	0	–	–	
140	–	2.46	2.44	–	0.813	–	–	
150	2.33	2.32	2.33	0	0.431	–	–	
160	–	2.24	2.23	–	0.446	–	–	

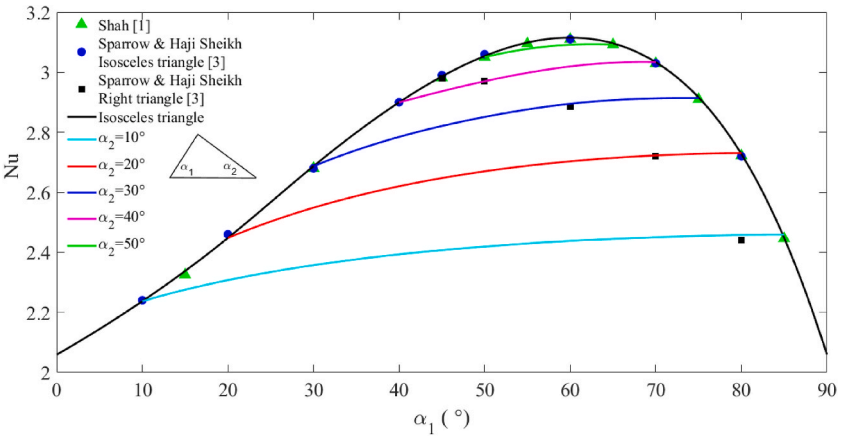

Fig. 6. Nusselt number for arbitrary triangles at $Br = 0$.

$$\delta I = \iint_R \left\{ \partial^2 T \Big/ \partial x^2 + \partial^2 T \Big/ \partial y^2 - 4w \Big/ W - (Br/W^2) \left((w/WA) \int \left((\partial w/\partial x)^2 + (\partial w/\partial y)^2 \right) dA - \left((\partial w/\partial x)^2 + (\partial w/\partial y)^2 \right) \right) \right\} \delta w dx dy = 0 \tag{32}$$

for temperature. By placing Eq. (29) in Eq. (31) we obtain:

$$\delta I = \int \left\{ \left(\partial^2 \left((a_1 + \ldots + a_{28} y^6) \psi \right) / \partial x^2 + \partial^2 \left((a_1 + \ldots + a_{28} y^6) \psi \right) / \partial y^2 \right) + 16 \right\} . \left\{ (a_1 + a_2 x + \ldots + a_{28} y^6) \delta \psi \right\} dA = 0 \tag{33}$$

Eq. (33) is the equation that must be solved to determine the unknown coefficients, which can be expanded as follows:

$$\begin{aligned} \delta I = {} & \delta a_1 \int \left\{ \left(\partial^2 \left((a_1 + \ldots + a_{28} y^6) \psi \right) / \partial x^2 + \partial^2 \left((a_1 + \ldots + a_{28} y^6) \psi \right) / \partial y^2 \right) + 16 \right\} \psi_1 dA \\ & + \delta a_2 \int \left\{ \left(\partial^2 \left((a_1 + \ldots + a_{28} y^6) \psi \right) / \partial x^2 + \partial^2 \left((a_1 + \ldots + a_{28} y^6) \psi \right) / \partial y^2 \right) + 16 \right\} \psi_2 dA \\ & + \delta a_3 \int \left\{ \left(\partial^2 \left((a_1 + \ldots + a_{28} y^6) \psi \right) / \partial x^2 + \partial^2 \left((a_1 + \ldots + a_{28} y^6) \psi \right) / \partial y^2 \right) + 16 \right\} \psi_3 dA + \ldots \\ & + \delta a_{28} \int \left\{ \left(\partial^2 \left((a_1 + \ldots + a_{28} y^6) \psi \right) / \partial x^2 + \partial^2 \left((a_1 + \ldots + a_{28} y^6) \psi \right) / \partial y^2 \right) + 16 \right\} \psi_{28} dA = 0 \end{aligned} \tag{34}$$

For Eq. (34) to be zero, each integral must be zero itself, and this means that:

$$\begin{aligned}
&\int \left(\partial^2\left((a_1+\ldots+a_{28}y^6)\psi\right)/\partial x^2+\partial^2\left((a_1+\ldots+a_{28}y^6)\psi\right)/\partial y^2\right)\psi_1 dA=-\int 16\psi_1 dA\\
&\int \left(\partial^2\left((a_1+\ldots+a_{28}y^6)\psi\right)/\partial x^2+\partial^2\left((a_1+\ldots+a_{28}y^6)\psi\right)/\partial y^2\right)\psi_2 dA=-\int 16\psi_2 dA\\
&\int \left(\partial^2\left((a_1+\ldots+a_{28}y^6)\psi\right)/\partial x^2+\partial^2\left((a_1+\ldots+a_{28}y^6)\psi\right)/\partial y^2\right)\psi_3 dA=-\int 16\psi_3 dA\\
&\vdots\\
&\int \left(\partial^2\left((a_1+\ldots+a_{28}y^6)\psi\right)/\partial x^2+\partial^2\left((a_1+\ldots+a_{28}y^6)\psi\right)/\partial y^2\right)\psi_{28} dA=-\int 16\psi_{28} dA
\end{aligned} \tag{35}$$

The unknown coefficients a_1 to a_{28} be obtained by solving simultaneous equations in Eq. (35), and by substituting them in Eq. (29), the value of w will be calculated. The same can be written for temperature by placing Eq. (30) in Eq. (32):

$$\begin{aligned}
&\int \left(\partial^2\left((a_1+\cdots+a_{28}y^6)\psi\right)/\partial x^2+\partial^2\left((a_1+\cdots+a_{28}y^6)\psi\right)/\partial y^2\right)\psi_1 dA=\\
&-\int\left\{(4w/W)+(Br/W^2)\left((w/WA)\int((\partial w/\partial x)^2+(\partial w/\partial y)^2)dA-\right.\right.\\
&\left.\left.((\partial w/\partial x)^2+(\partial w/\partial y)^2)\right)\right\}\psi_1 dA\\
&\int \left(\partial^2\left((a_1+\cdots+a_{28}y^6)\psi\right)/\partial x^2+\partial^2\left((a_1+\cdots+a_{28}y^6)\psi\right)/\partial y^2\right)\psi_2 dA=\\
&-\int\left\{(4w/W)+(Br/W^2)\left((w/WA)\int((\partial w/\partial x)^2+(\partial w/\partial y)^2)dA-\right.\right.\\
&\left.\left.((\partial w/\partial x)^2+(\partial w/\partial y)^2)\right)\right\}\psi_2 dA\\
&\int \left(\partial^2\left((a_1+\cdots+a_{28}y^6)\psi\right)/\partial x^2+\partial^2\left((a_1+\cdots+a_{28}y^6)\psi\right)/\partial y^2\right)\psi_3 dA=\\
&-\int\left\{(4w/W)+(Br/W^2)\left((w/WA)\int((\partial w/\partial x)^2+(\partial w/\partial y)^2)dA-\right.\right.\\
&\left.\left.((\partial w/\partial x)^2+(\partial w/\partial y)^2)\right)\right\}\psi_3 dA\\
&\vdots\\
&\int \left(\partial^2\left((a_1+\cdots+a_{28}y^6)\psi\right)/\partial x^2+\partial^2\left((a_1+\cdots+a_{28}y^6)\psi\right)/\partial y^2\right)\psi_{28} dA=\\
&-\int\left\{(4w/W)+(Br/W^2)\left((w/WA)\int((\partial w/\partial x)^2+(\partial w/\partial y)^2)dA-\right.\right.\\
&\left.\left.((\partial w/\partial x)^2+(\partial w/\partial y)^2)\right)\right\}\psi_{28} dA
\end{aligned} \tag{36}$$

As in Eq. (35), the unknown coefficients a_1 to a_{28} are obtained by solving the simultaneous equations in Eq. (36), and by placing them in Eq. (30), the temperature can be obtained.

4. Results and discussion

Herein, the results of the solution of momentum and energy equations for an incompressible fluid inside triangular channels were obtained using the Ritz method. The domain of equations' solution that involves any triangular section is illustrated in Fig. 1. Angles α_1 and α_2 are sufficient to determine the geometrical configuration of the triangle. The results are presented as Nusselt number, Poiseuille number, $C_f Re$, and dimensionless temperature contour. The findings are compared with previous studies for isosceles and right triangles. The velocity equation for the equilateral triangular cross-section is given in "*Viscous Fluid Flow*" by Papanastasiou et al. [29]. Fig. 3 compares the dimensionless velocity profile contour in the equilateral triangular section for the equation presented in Ref. [29] (Fig. 3a) and that of the current study (Fig. 3b).

According to Fig. 3, the velocity value at the walls is zero, which satisfies the wall boundary conditions. It is also clear that the velocity value is the highest at the center of the triangle. Therefore, according to the figure, our solution agrees with the reported results. Table 1 compares the Poiseuille number obtained in the current study with those of previous studies. The amounts of error between the results are also presented in Table 1. The result shows a more significant error in slender triangles than other triangular sections.

ϵ_1, ϵ_2, ϵ_3 and ϵ_4 are the percentage of error between the results of Ref. [1], Ref. [3], Ref. [30] (isosceles triangle), Ref. [3] (right triangle), and the analytical solution obtained in the current study, respectively.

Fig. 4 shows the values of the Poiseuille number for any triangular cross-section, which obtained in term of α_1 and α_2. The remarkable agreement of the current study with those shown in several previous studies is outstanding, which provides us sufficient confidence about validating our solution using the Ritz method. According to the figure, the Poiseuille number varies from 48 to 53.3, and it can be concluded that the wider triangles have a greater value of the Poiseuille number. Among a set of triangles that have the same angle α_2, the maximum Poiseuille number is related to an isosceles where α_2 is the vertex angle. Also, the maximum Poiseuille number between all the triangles belongs to the equilateral triangle. The pressure drop and fluid head loss can be calculated using the data of Fig. 4 and having the information of fluid and flow.

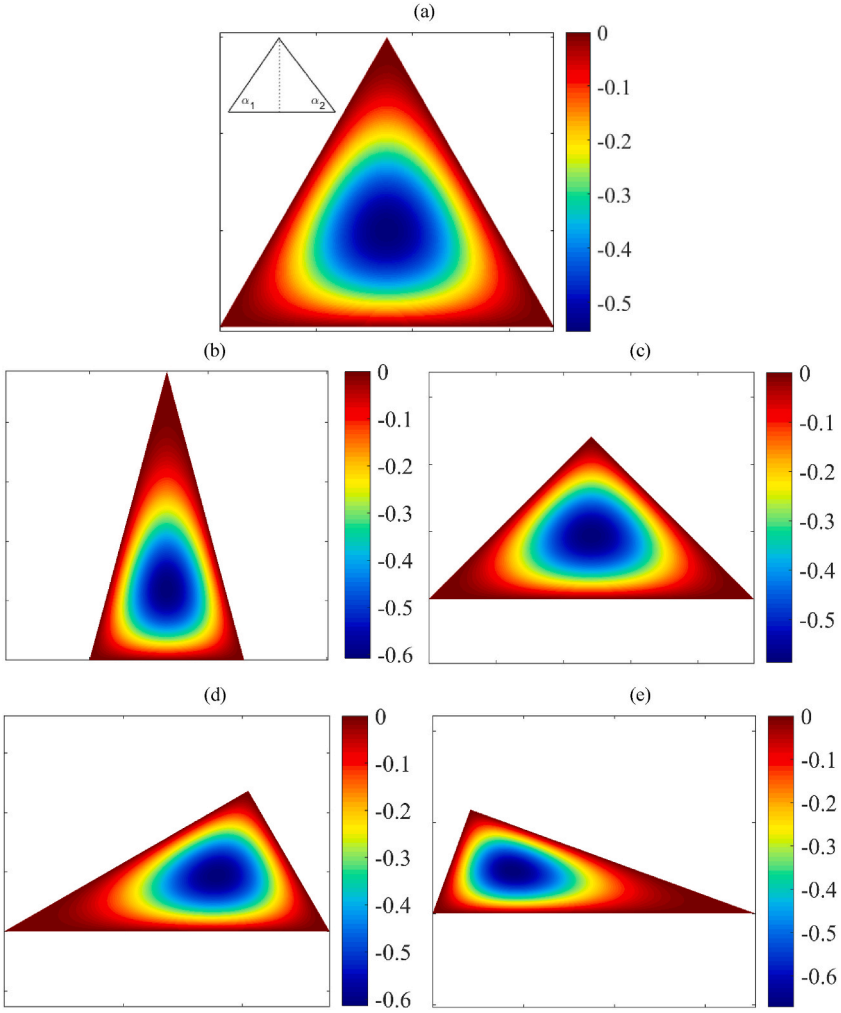

Fig. 7. Temperature distribution contours ($Br = 0$) for (a) equilateral triangle (isosceles triangle $\alpha_1 = \alpha_2 = 60$), (b) isosceles triangle $\alpha_1 = \alpha_2 = 75$, (c) isosceles triangle $\alpha_1 = \alpha_2 = 45$, (d) right triangle $\alpha_1 = 30$ and $\alpha_2 = 60$, and (e) right triangle $\alpha_1 = 70$ and $\alpha_2 = 20$.

Fig. 5 represents the variation of C_f.Re in equilateral (Fig. 5a), isosceles (Fig. 5b and c), and right triangular sections (Fig. 5d and e). According to the figure, the position of the maximum values of the skin friction coefficient is far from the acute angle and close to the obtuse angle. In an equilateral triangle, this maximum value is located exactly in the middle of each side. The presence of the acute angle has a notable impact on the flow within the triangular duct. The fluid flow and heat transfer at rounded corner triangles were studied by Kumar et al. [31], which shows that the flow is stagnant at sharp corners. Therefore, based on Eq. (21), the skin friction coefficient equals zero at the corners of the triangle. Fig. 5 shows that the skin friction coefficient is zero at the corners of triangles.

Table 2 presents the Nusselt number comparison between the present study and previous data. The table shows that the results are consistent with the reported results.

ϵ_1, ϵ_2, and ϵ_3 are the percentage of error between the results of Ref. [1], Ref. [3] (isosceles triangle), Ref. [3] (right triangle), and the analytical solution obtained in the current study, respectively.

Here, forced convection heat transfer was studied in two modes: I) Thermal analysis without viscous dissipation and II) Thermal analysis with considering the viscous dissipation. To study the case *I*, the Brinkman number in the energy equation was assumed to be zero ($Br = 0$). Considering a constant heat flux to the walls, heat transfer occurs from the walls to the fluid. Fig. 6 shows the Nusselt number for any triangular cross-section. The results reported by Shah [1] and Sparrow and Haji-Sheikh [3] for isosceles and right triangular cross-sections are also presented in this figure. According to the figure, it can be found that higher values of Nusselt number are related to the wider triangles. The maximum Nusselt number occurs at the equilateral triangle. Furthermore, the maximum Nusselt number between a set of triangles with a similar angle α_2 is related to an isosceles where α_2 is the vertex angle. The maximum Nusselt number among all triangles also belongs to the equilateral triangle

It is evident that geometries related to a triangle with a 0° angle and a triangle with two 90° angles do not exist. These results are presented from Shah's [1] study in Figs. 4 and 6 to be employed for interpolating and obtaining values for a certain geometry from a

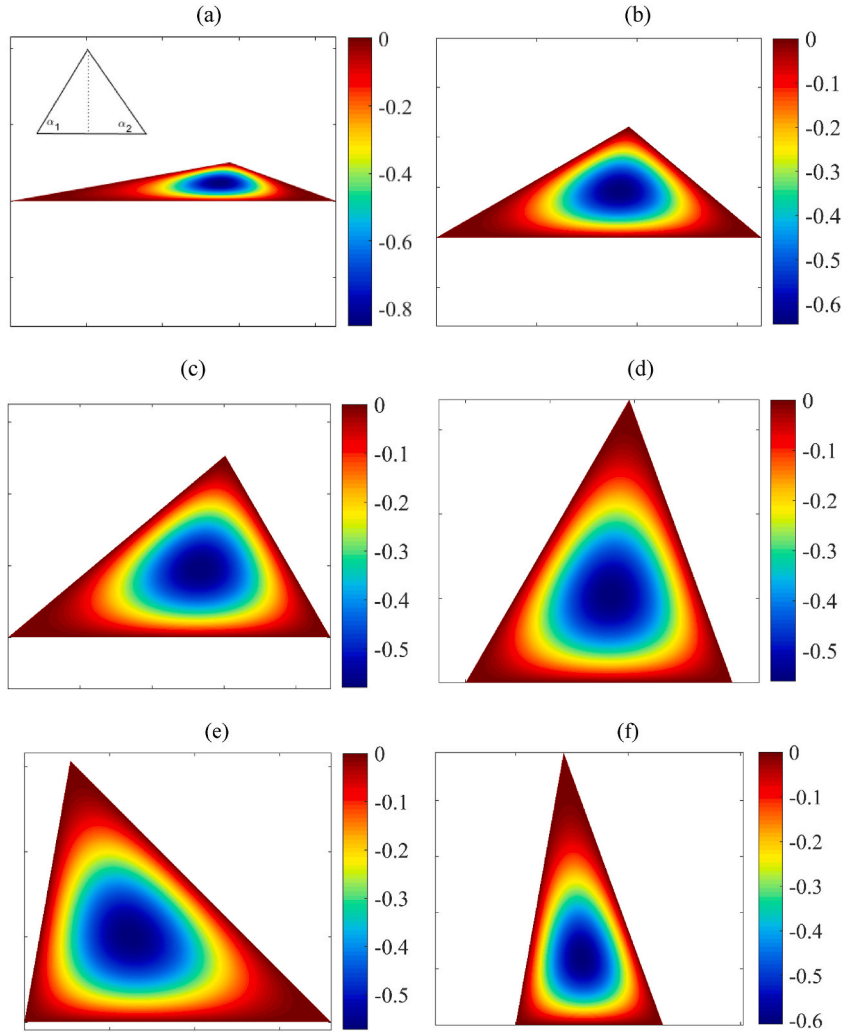

Fig. 8. Temperature distribution contours for arbitrary triangle ($Br = 0$) (a) $\alpha_1 = 10$, $\alpha_2 = 20$, (b) $\alpha_1 = 30$, $\alpha_2 = 40$, (c) $\alpha_1 = 40$, $\alpha_2 = 60$, (d) $\alpha_1 = 60$, $\alpha_2 = 70$, (e) $\alpha_1 = 80$, $\alpha_2 = 45$ and (f) $\alpha_1 = 80$, $\alpha_2 = 70$.

triangle. The dimensionless temperature distribution for different triangular sections is depicted in Figs. 7 and 8. Fig. 7 incorporates equilateral (Fig. 7a), isosceles (Fig. 7b and c), and right triangular sections (Fig. 7d and e), and Fig. 8a–f involves several arbitrary triangular geometries. Evidently, the dimensionless temperature is zero on the boundaries and the highest at the walls. According to Eq. (4), the negative temperature values inside the duct indicate that the fluid temperature is lower than the walls.

According to Eq. (12), the dimensionless dissipation component of the energy equation (φ) is given in Eq. (37):

$$\varphi = \left(1 / W^2\right)\left((\partial w/\partial x)^2 + (\partial w/\partial y)^2\right). \tag{37}$$

The dissipation distribution contour for different triangular cross-sections is shown in Figs. 9 and 10. Fig. 9 contains equilateral (Fig. 9a), isosceles (Fig. 9b and c), and right-angled triangle sections (Fig. 9d and e), and Fig. 10a–f contain several arbitrary triangle geometries. Regarding the obtained results of the skin friction coefficient mentioned above, it is expected that the highest value of dissipation occurs on the walls and at the points where C_f is maximum. The main reason is that stress is at its highest level at these points. The dissipation values also equal zero in the corners and centers of triangles. Therefore, it can be seen that the narrower the triangle, the more its maximum dissipation.

The Integration of the Dissipation Distribution (IDD), which is a constant, can be written as Eq. (38). This number is varied for different types of triangles. The IDD for arbitrary triangles has been shown in Fig. 11.

$$\int \varphi dA = \left(1 / W^2\right) \int \left((\partial w/\partial x)^2 + (\partial w/\partial y)^2\right) dA. \tag{38}$$

According to Fig. 11, it can be obtained that the wider the triangle, the lower the value of its IDD. It also observed that the variation

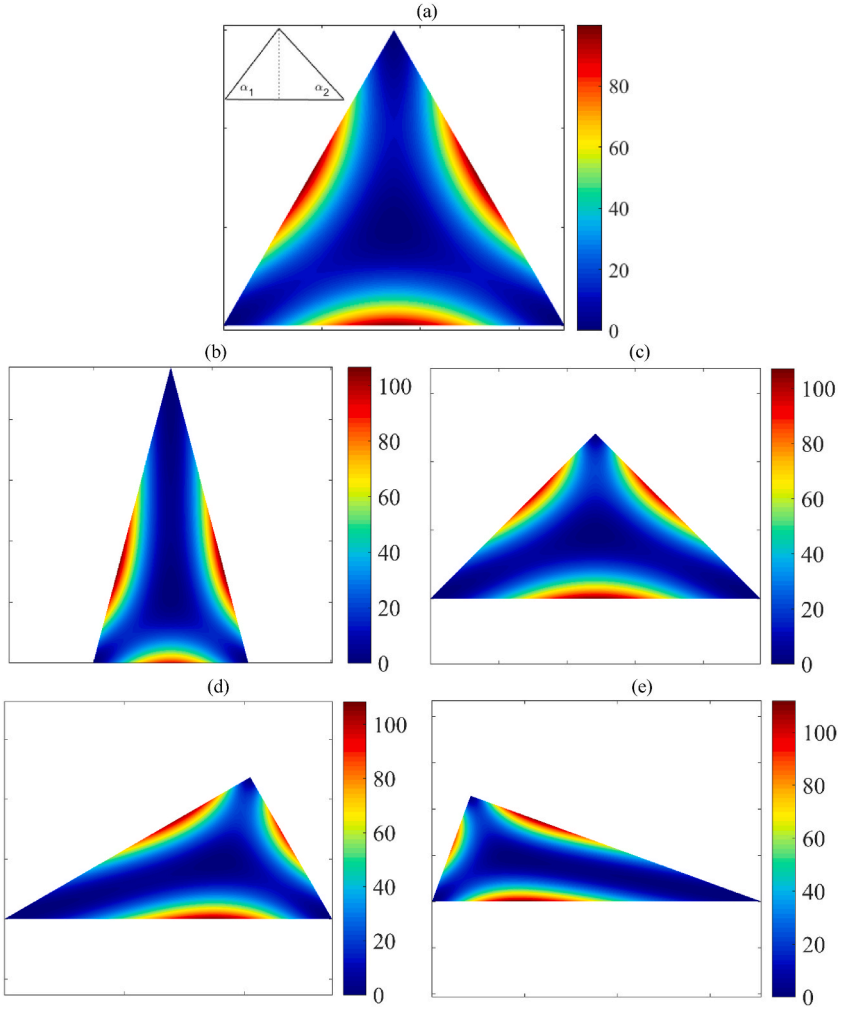

Fig. 9. Dissipation distribution contours for (a) equilateral triangle (isosceles triangle $\alpha_1 = \alpha_2 = 60$), (b) isosceles triangle $\alpha_1 = \alpha_2 = 75$, (c) isosceles triangle $\alpha_1 = \alpha_2 = 45$, (d) right triangle $\alpha_1 = 30$ and $\alpha_2 = 60$, and (e) right triangle $\alpha_1 = 70$ and $\alpha_2 = 20$.

range of IDD for all triangles which have the same (α_2) angle is very small, and this variation range is reduced by enhancing the angle. Among all triangles that have the identical angle (α_2), the least value is related to the isosceles triangle with (α_2) at the apex, and the minimum quantity of IDD belongs to the equilateral triangle. As mentioned, according to Fig. 4, the equilateral triangle has the highest value of the Poiseuille number (f.Re) among all triangle shapes. This indicates that the Reynolds number increases for a specific pressure gradient as the cross-section widens, resulting in a larger Poiseuille number, unlike the IDD number.

For $Br \neq 0$, viscous dissipation influences heat transfer and the duct's temperature distribution. The Brinkman number can vary from -∞ to +∞. Norouzi et al. [22] presented an equation to calculate the Nusselt number in equilateral triangular sections. Figs. 12 and 13, respectively, compare the Nusselt number and temperature distribution of the current study with those obtained by Norouzi et al. [22] for different Brinkman numbers. Comparison of obtained results with available data indicates the accuracy and reliability of the solution.

Positive and negative Nusselt numbers are observed for different Brinkman numbers in Fig. 12. The critical Brinkman numbers occur where the sign of Nusselt number changes from positive to negative or vice versa. This critical number for an equilateral triangle equals −0.275 (Fig. 13e and f). In addition, Fig. 13a–d shows the wall cooling cases, and Fig. 13g–l shows the wall heating cases. Tables 3 and 4 present Nusselt numbers for isosceles and right triangles for different Brinkman numbers and the critical Brinkman number for each section.

The Nusselt number for different Brinkman numbers for any triangular section is presented in Fig. 14. For $Br \neq 0$, by increasing the triangle size, the Nusselt number increases in the heating cases (Fig. 14d–f) and decreases in the cooling cases (Fig. 14a–c). Moreover, the maximum Nusselt number for a set of triangles with a similar angle α_2 in heating cases, and also the minimum Nusselt number among a set of triangles with a similar angle α_2 in cooling cases are related to an isosceles triangle where α_2 is the apex angle. In addition, among any triangular section, the maximum Nusselt number between the heating cases and the minimum Nusselt number between the cooling cases for different Brinkman numbers belongs to the equilateral triangle. Figs. 15 and 16 show the dimensionless

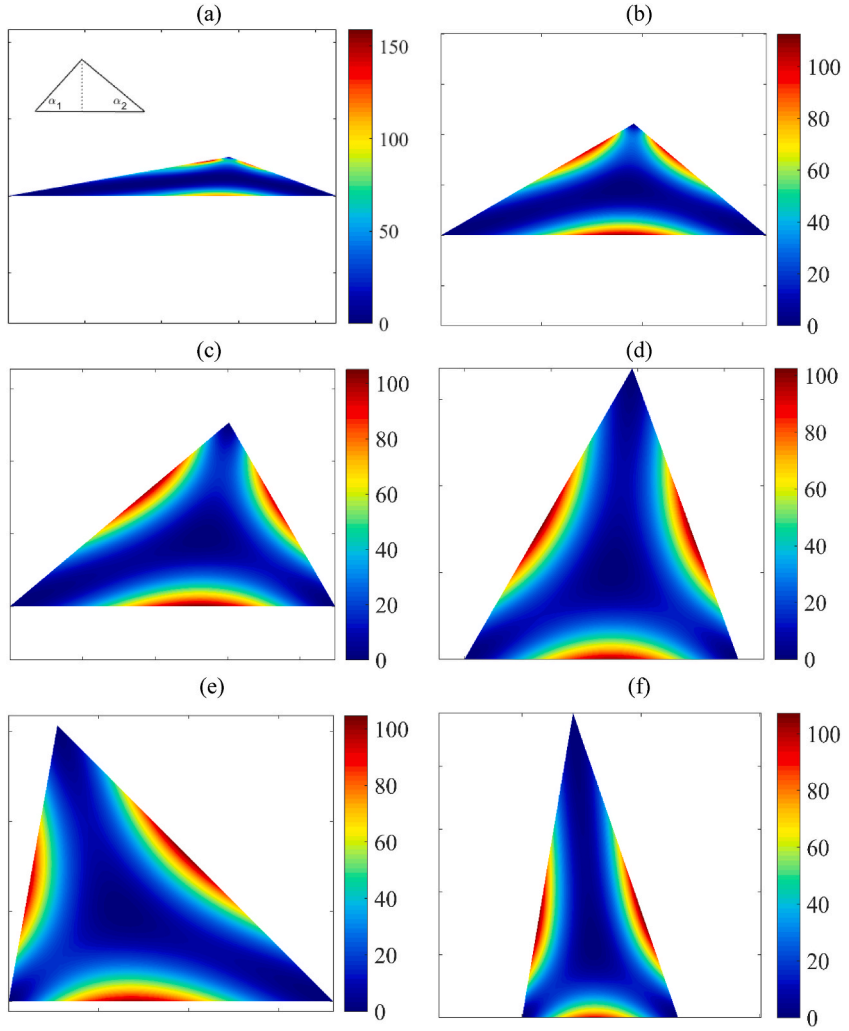

Fig. 10. Dissipation distribution contours for arbitrary triangle (a) $\alpha_1 = 10$, $\alpha_2 = 20$, (b) $\alpha_1 = 30$, $\alpha_2 = 40$, (c) $\alpha_1 = 40$, $\alpha_2 = 60$, (d) $\alpha_1 = 60$, $\alpha_2 = 70$, (e) $\alpha_1 = 80$, $\alpha_2 = 45$ and (f) $\alpha_1 = 80$, $\alpha_2 = 70$.

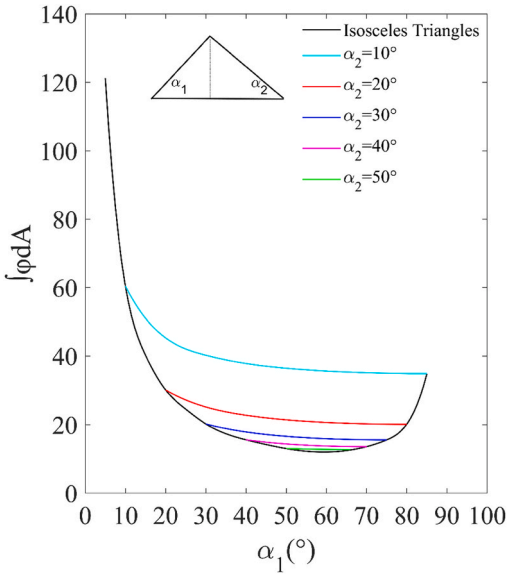

Fig. 11. The integration of the dissipation distribution for arbitrary triangles.

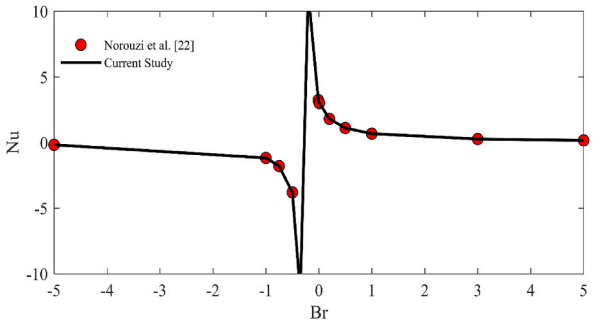

Fig. 12. Nusselt number for different Brinkman numbers in an equilateral triangle.

temperature distribution at the critical points of various triangular sections of the Brinkman number. Fig. 15 represents equilateral (Fig. 15a), isosceles (Fig. 15b and c) and right-angled triangle sections (Fig. 15d and e), and Fig. 16a–f represent several arbitrary triangle geometries.

Figs. 12 and 14 illustrate that the Nusselt number tends zero when the Brinkman number approaches to $\pm\infty$. Moreover, the *Nu* tends to ∞ when the Br approaches the critical Brinkman number. According to Figs. 12–14, the heat flux is positive for $0<Br<+\infty$ (wall heating case). In other words, the heat flux applied to the wall overcomes one produced by viscous dissipation; the heat transfer occurs from the wall to the fluid.

On the other hand, the heat flux sign is negative for $-\infty<Br<Br_c$ (wall cooling case), which means the amount of heat flux produced by viscous dissipation overcomes the one applied to the wall, and the heat transfer occurs from the core of the flow to the wall. The change in the direction of heat transfer from the flow to the wall can explain the occurrence of negative Nusselt numbers in this area. In fact, as seen in the Brinkman number formulation, the Brinkman number represents the proportion between the heat produced by viscous dissipation and the heat produced by molecular conduction. Decreasing the viscosity reduces the contribution of thermal conductivity. As a result, for both cooling and heating cases, a higher value of the Brinkman number leads to a lower Nusselt number. The critical Brinkman number (Br_c) is the point at which the direction of heat transfer changes. At this point, the difference between the mean temperature of the fluid, under the influence of viscous dissipation, and the wall temperature becomes negligible, causing *Nu* to tend towards infinite.

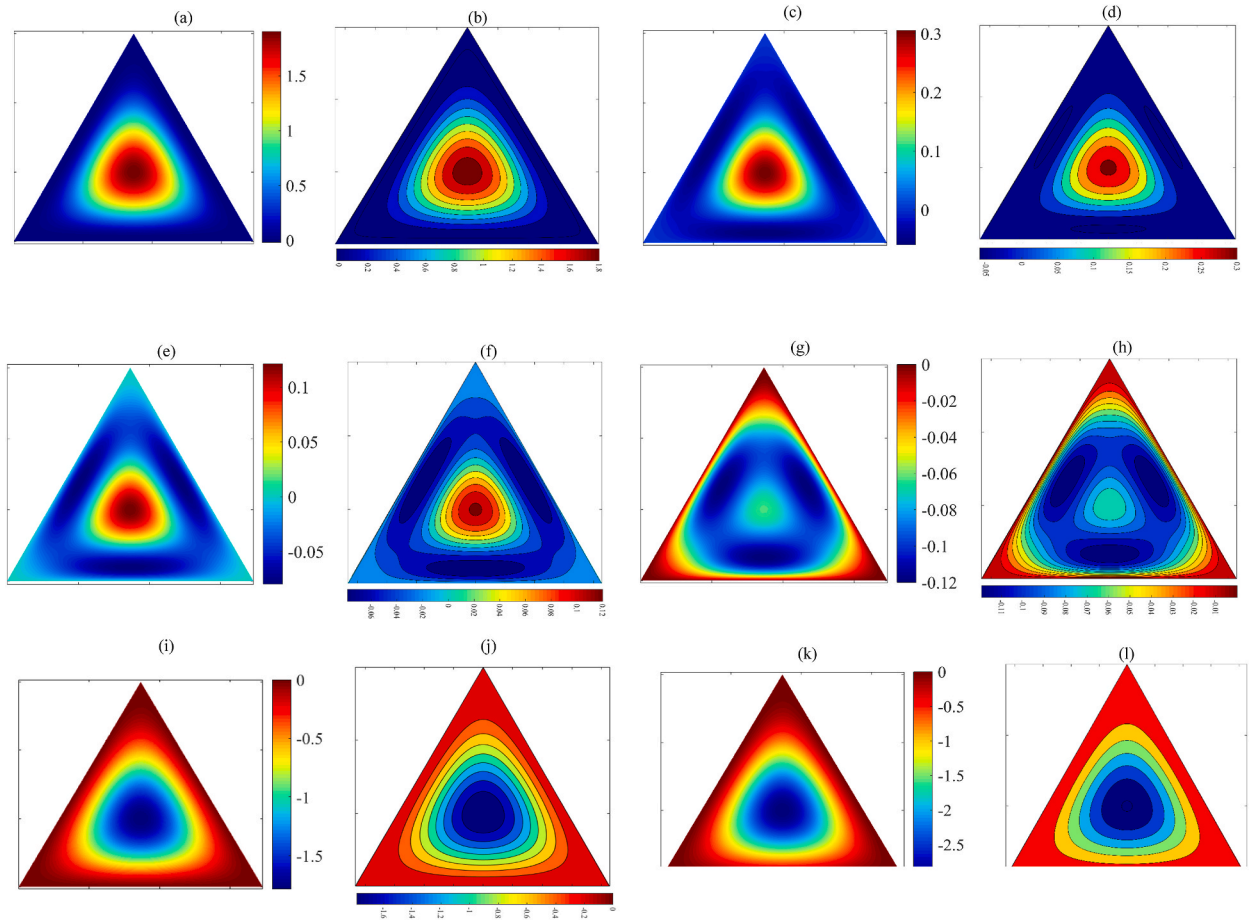

Fig. 13. Temperature distribution contours for an equilateral triangle (Br≠0) (a) current study $Br = -1$, (b) Ref. [22] $Br = -1$, (c) current study $Br = -0.35$, (d) Ref. [22] $Br = -0.35$, (e) current study $Br = -0.275$, (f) Ref. [22] $Br = -0.275$, (g) current study $Br = -0.2$ and (h) Ref. [22] $Br = -0.2$, (i) current study $Br = 0.5$, (j) Ref. [22] $Br = 0.5$, (k) current study $Br = 1$, (l) Ref. [22] $Br = 1$.

Table 3
Nusselt number for different Brinkman numbers in isosceles triangles.

Brinkman numbers	Nusselt number for Isosceles triangle 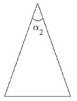												
	$\alpha = 10$	$\alpha = 20$	$\alpha = 30$	$\alpha = 40$	$\alpha = 50$	$\alpha = 60$	$\alpha = 70$	$\alpha = 80$	$\alpha = 90$	$\alpha = 110$	$\alpha = 130$	$\alpha = 150$	$\alpha = 170$
−5	−0.158	−0.169	−0.175	−0.179	−0.181	−0.182	−0.181	−0.18	−0.177	−0.17	−0.162	−0.152	−0.144
−1	−1.066	−1.12	−1.152	−1.173	−1.184	−1.19	−1.184	−1.18	−1.164	−1.128	−1.08	−1.024	−0.982
−0.75	−1.66	−1.723	−1.77	−1.8	−1.81	−1.813	−1.81	−1.8	−1.784	−1.738	−1.674	−1.6	−1.542
−0.5	−3.77	−3.8	−3.81	−3.826	−3.835	−3.84	−3.833	−3.826	−3.814	−3.78	−3.726	−3.651	−3.586
−0.2	7.229	8.766	9.92	10.724	11.18	11.32	11.2	10.88	10.409	9.212	7.92	6.778	6.065
−0.01	2.538	2.825	3.022	3.146	3.212	3.232	3.215	3.168	3.096	2.9	2.658	2.413	2.243
0.01	2.376	2.637	2.816	2.928	2.99	3	2.991	2.948	2.883	2.7046	2.484	2.26	2.103
0.2	1.478	1.615	1.709	1.77	1.797	1.8	1.798	1.776	1.743	1.65	1.533	1.41	1.322
0.5	0.926	1	1.054	1.086	1.1029	1.108	1.103	1.091	1.073	1.021	0.955	0.884	0.833
1	0.57	0.614	0.643	0.662	0.671	0.674	0.671	0.664	0.654	0.625	0.587	0.546	0.516
3	0.225	0.24	0.251	0.258	0.261	0.262	0.261	0.259	0.255	0.245	0.23	0.215	0.204
5	0.14	0.15	0.156	0.16	0.162	0.163	0.162	0.161	0.159	0.152	0.144	0.134	0.127
Br_c	−0.302	−0.29	−0.283	−0.278	−0.276	−0.275	−0.276	−0.278	−0.28	−0.287	−0.296	0.305	−0.312

Table 4
Nusselt number for different Brinkman numbers in right triangles.

Brinkman numbers	Nusselt number for right triangle			
	$\alpha = 10$	$\alpha = 20$	$\alpha = 30$	$\alpha = 40$
−5	−0.159	−0.168	−0.174	−0.177
−1	−1.074	−1.117	−1.148	−1.162
−0.75	−1.677	−1.726	−1.763	−1.781
−0.5	−3.816	−3.79	−3.804	−3.813
−0.2	7.179	8.707	9.78	10.338
−0.01	2.541	2.82	2.998	3.086
0.01	2.38	2.632	2.794	2.873
0.2	1.483	1.614	1.698	1.738
0.5	0.93	1	1.048	1.07
1	0.573	0.614	0.64	0.652
3	0.226	0.24	0.25	0.255
5	0.141	0.15	0.155	0.158
Br_c	−0.304	−0.29	−0.283	−0.28

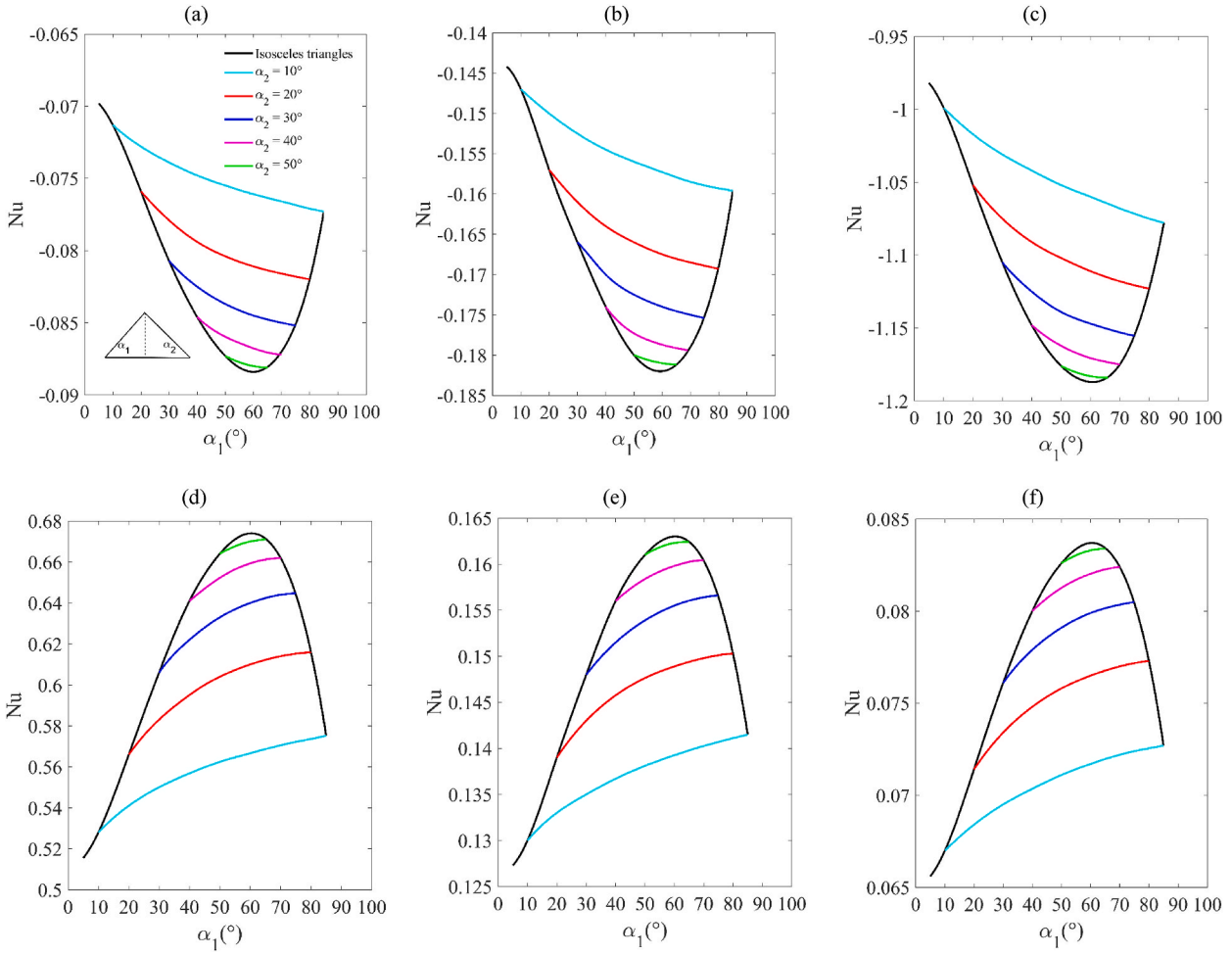

Fig. 14. Nusselt number for an arbitrary triangle (a) $Br = -10$, (b) $Br = -5$, (c) $Br = -1$, (d) $Br = 1$, (e) $Br = 5$, (f) $Br = 10$.

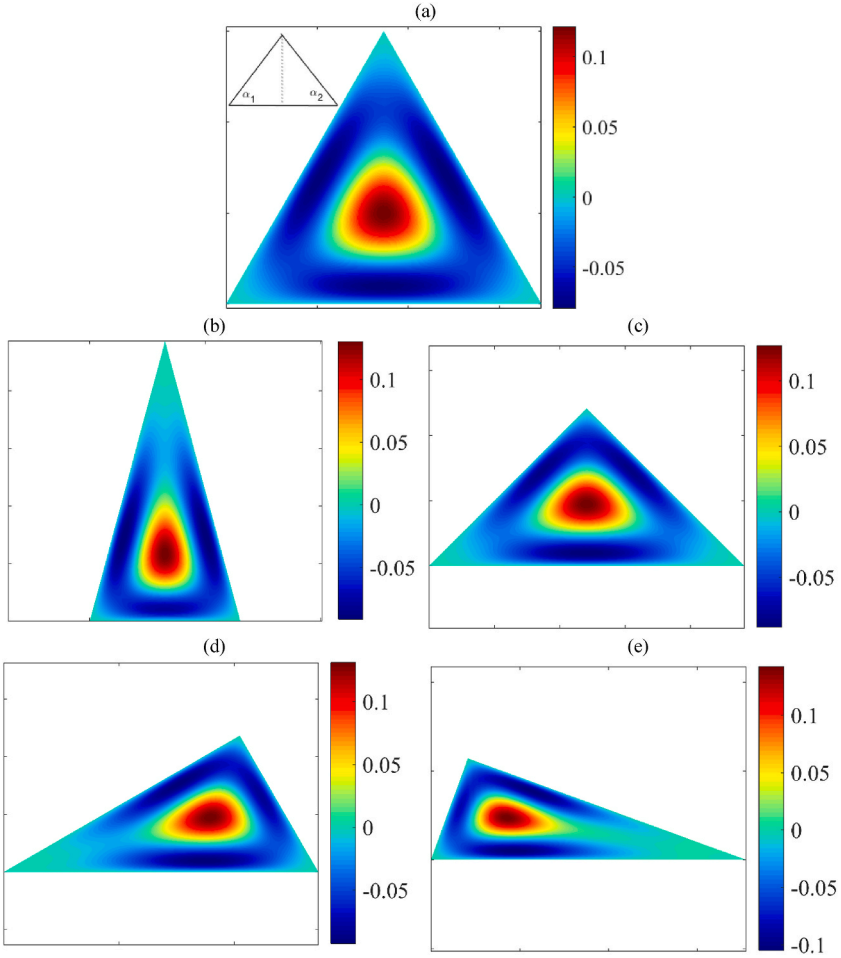

Fig. 15. Temperature distribution contours for (a) an equilateral triangle $Br = -0.275$ (isosceles triangle $\alpha_1 = \alpha_2 = 60$), (b) isosceles triangle $Br = -0.283$, $\alpha_1 = \alpha_2 = 75$, (c) isosceles triangle $Br = -0.28$, $\alpha_1 = \alpha_2 = 45$, (d) right triangle $Br = -0.284$, $\alpha_1 = 30$ and $\alpha_2 = 60$, and (e) right triangle $Br = -0.29$, $\alpha_1 = 70$ and $\alpha_2 = 20$.

5. Concluding remarks

In this paper, the flow and heat transfer through the arbitrarily-shaped triangular ducts, with and without viscous dissipation, is solved for the first time using the Ritz method under a constant heat flux boundary condition. When viscous dissipation is considered, the heat transfer solution is divided into wall cooling cases ($Br < Br_c$) and wall heating cases ($Br > Br_c$), where Br_c represents the critical Brinkman number. At this point, the difference between the fluid's mean and wall temperatures was minimal, and the Nusselt number tended to be infinite. According to the results, Br_c was the point of the change in the sign of Nusselt number, which meant a shift in the direction of heat transfer. Generally, both in the cooling and heating modes, Nusselt number decreased with increasing the Brinkman number. Among a set of triangles, with the similar angle α_2, the following terms:

- The maximum value of the Poiseuille number,
- The highest Nusselt number value at $Br = 0$,
- The minimum value of the integration of dissipation distribution,
- The maximum value of the Nusselt number for the wall heating mode,
- The minimum value of the Nusselt number for the wall cooling mode

belongs to an isosceles triangle where α_2 is the apex angle. Between types of triangles, the items mentioned above belong to the equilateral triangle.

According to the verification of the present study, the high accuracy of the results in the current study is evident. However, the validity of an analytical solution is determined by comparing it with experimental and numerical studies. Researchers can solve this problem for various triangle shapes using numerical and experimental methods and compare their findings with the results of this

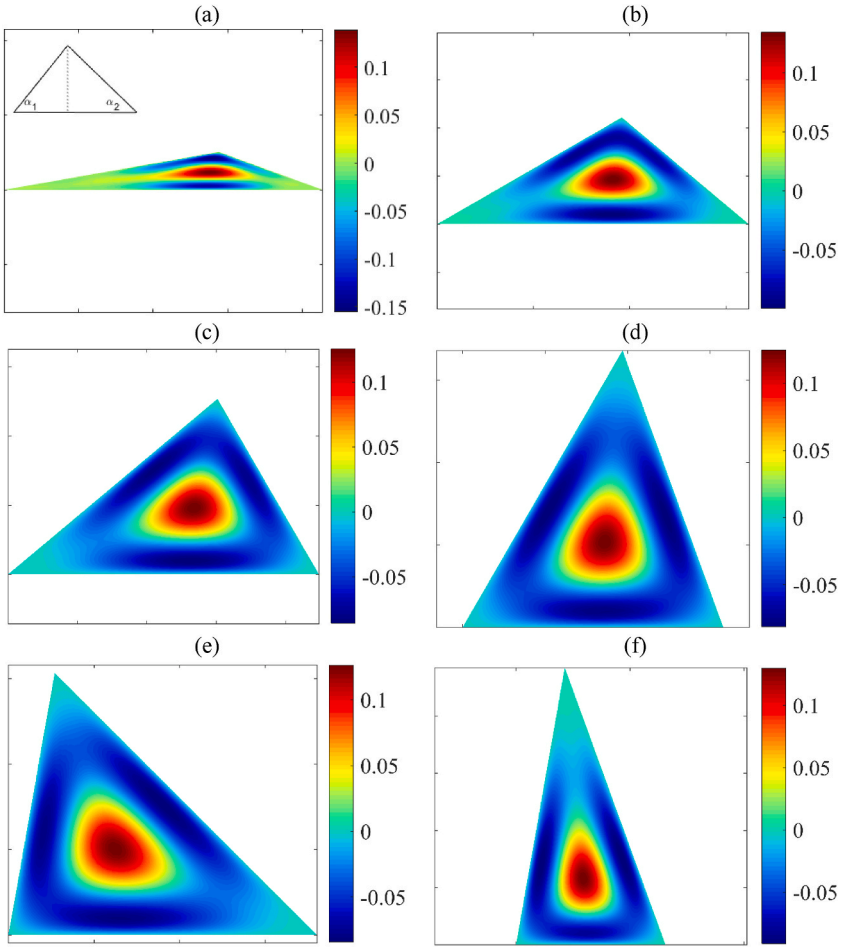

Fig. 16. Temperature distribution contours for an arbitrary triangle (a) $Br = -0.306$, $\alpha_1 = 10$, $\alpha_2 = 20$, (b) Br $= -0.288$, $\alpha_1 = 30$, $\alpha_2 = 40$, (c) $Br = -0.279$, $\alpha_1 = 40$, $\alpha_2 = 60$, (d) $Br = -0.277$, $\alpha_1 = 60$, $\alpha_2 = 70$, (e) $Br = -0.279$, $\alpha_1 = 80$, $\alpha_2 = 45$ and (f) $Br = -0.28$, $\alpha_1 = 80$, $\alpha_2 = 70$.

study. This would also enhance the credibility of the current study. Furthermore, future research can address the issue of heat transfer through ducts with arbitrary triangular cross-sections for other fluids, such as non-Newtonian fluids or nanofluids. Other thermal boundary conditions, such as a constant wall temperature, can be considered for future works.

Data availability

The corresponding author is ready to provide the data and models supporting the findings of this study upon a reasonable request.

Additional information

No additional information is available for this paper.

CRediT authorship contribution statement

Amirhossein Hajiaghaei Tabalvandani: Writing – review & editing, Writing – original draft, Methodology, Investigation, Formal analysis, Data curation, Conceptualization. **Mahmood Norouzi:** Writing – review & editing, Validation, Supervision, Methodology, Investigation, Conceptualization. **Mohammad Hassan Kayhani:** Writing – review & editing, Visualization, Validation, Methodology, Data curation. **Amir Komeili Birjandi:** Writing – review & editing, Software, Methodology, Investigation, Data curation. **Amin Emamian:** Writing – review & editing, Visualization, Validation, Investigation. **Mirae Kim:** Writing – review & editing, Validation, Supervision, Funding acquisition. **Kyung Chun Kim:** Writing – review & editing, Resources, Project administration, Funding acquisition, Conceptualization.

Declaration of competing interest

The authors declare that they have no known competing financial interests or personal relationships that could have appeared to influence the work reported in this paper.

Acknowledgment

This research received support from the Brain Pool Program through the National Research Foundation of Korea (NRF), funded by the Ministry of Science and ICT (NRF-2022H1D3A2A01091637). Additionally, financial backing was provided by the National Research Foundation of Korea (NRF) through grants from the Korean government (MSIT) (No. 2020R1A5A8018822, No. 2021R1C1C2009287). The authors extend their gratitude to the Shahrood University of Technology for the financial support.

References

[1] R. Shah, Laminar flow friction and forced convection heat transfer in ducts of arbitrary geometry. International Journal of Heat and Mass Transfer 18 (7–8) (1975) 849–862.
[2] E. Sparrow, Laminar flow in isosceles triangular ducts, AIChE J. 8 (5) (1962) 599–604.
[3] E. Sparrow, A. Haji-Sheikh, Laminar heat transfer and pressure drop in isosceles triangular, right triangular, and circular sector ducts, Journal of Heat Transfer 87 (3) (1965) 426–427.
[4] F. Schmidt, M. Newell, Heat transfer in fully developed laminar flow through rectangular and isosceles triangular ducts. International journal of heat and mass transfer 10 (8) (1967) 1121–1123.
[5] J. Aparecido, R. Cotta, Laminar thermally developing flow inside right-angularly triangular ducts, Appl. Sci. Res. 49 (4) (1992) 355–368.
[6] S.G. Etemad, A. Mujumdar, R. Nassef, Simultaneously developing flow and heat transfer of non-Newtonian fluids in equilateral triangular duct, Appl. Math. Model. 20 (12) (1996) 898–908.
[7] S. Chen, et al., Numerical prediction of laminar forced convection in triangular ducts with unstructured triangular grid method, Numer. Heat Tran. Part A: Applications 38 (2) (2000) 209–224.
[8] C.L. Chaves, et al., Forced convection heat transfer to power-law non-Newtonian fluids inside triangular ducts, Heat Tran. Eng. 25 (7) (2004) 23–33.
[9] K. Hooman, A. Haji-Sheikh, Analysis of heat transfer and entropy generation for a thermally developing Brinkman–Brinkman forced convection problem in a rectangular duct with isoflux walls. International journal of heat and mass transfer 50 (21–22) (2007) 4180–4194.
[10] L.-Z. Zhang, Laminar flow and heat transfer in plate-fin triangular ducts in thermally developing entry region. International journal of heat and mass transfer 50 (7–8) (2007) 1637–1640.
[11] S. Ray, D. Misra, Laminar fully developed flow through square and equilateral triangular ducts with rounded corners subjected to H1 and H2 boundary conditions. International Journal of Thermal Sciences 49 (9) (2010) 1763–1775.
[12] C. Wang, Exact solutions for starting and oscillatory flows in an equilateral triangular duct, J. Fluid Eng. (2016) 138, 8.
[13] C. Wang, Benchmark solutions for slip flow and H1 heat transfer in rectangular and equilateral triangular ducts, J. Heat Tran. (2013) 135, 2.
[14] C. Wang, Stokes flow in a curved duct–A Ritz method, Comput. Fluids 53 (2012) 145–148.
[15] C. Wang, Slip flow and constant flux heat transfer in isosceles triangular ducts. Journal of Thermophysics and Heat Transfer 31 (1) (2017) 69–77.
[16] C. Wang, Ritz method for oscillatory flow in ducts. International journal for numerical methods in fluids 67 (5) (2011) 609–615.
[17] H. Karabulut, D. Ipci, C.J.A.T.E. Cinar, Numerical solution of fully developed heat transfer problem with constant wall temperature and application to isosceles triangle and parabolic ducts 102 (2016) 115–124.
[18] Y.M. Hung, Analytical study on forced convection of nanofluids with viscous dissipation in microchannels, Heat Tran. Eng. 31 (14) (2010) 1184–1192.
[19] Y.-M. Hung, C. Tso, Effects of viscous dissipation on fully developed forced convection in porous media. International Communications in Heat and Mass Transfer 36 (6) (2009) 597–603.
[20] O. Aydin, Effects of viscous dissipation on the heat transfer in forced pipe flow. Part 1: both hydrodynamically and thermally fully developed flow, Energy Convers. Manag. 46 (5) (2005) 757–769.
[21] O. Aydın, M. Avcı, Laminar forced convection with viscous dissipation in a Couette–Poiseuille flow between parallel plates, Appl. Energy 83 (8) (2006) 856–867.
[22] M. Norouzi, et al., An exact solution for fluid flow and heat convection through triangular ducts considering the viscous dissipation. AUT journal of mechanical engineering 3 (2) (2019) 197–204.
[23] H.A. Kose, A. Yildizeli, S.J.A.T.E. Cadirci, Parametric study and optimization of microchannel heat sinks with various shapes. 211 (2022) 118368.
[24] A. Moradikazerouni, et al., Comparison of the effect of five different entrance channel shapes of a micro-channel heat sink in forced convection with application to cooling a supercomputer circuit board. 150 (2019) 1078–1089.
[25] A. Bejan. Convection heat transfer, John Wiley & Sons, Inc, Hoboken, Ontario, 2013.
[26] S.G. Kandlikar, SINGLE-PHASE liquid flow in minichannels, Heat transfer and fluid flow in minichannels and microchannels (2006) 87.
[27] M. Norouzi, A. Emamian, M.J.J.o.E.M. Davoodi, A new mathematical technique for analysis of internal viscoplastic flows through rectangular ducts. 127 (1) (2021) 1–26.
[28] V.S. Arpaci. Conduction heat transfer, Addison-Wesley, Publishing Company, London, 1966.
[29] T. Papanastasiou, G. Georgiou, A.N. Alexandrou. Viscous fluid flow, CRC Press, London, 2000.
[30] F.M. White. Viscous fluid flow, 3rd Edition, McGraw, Hill, Boston, 2006.
[31] R. Kumar, et al., Effect of dimple intrusions and curvature radius of rounded corner triangular duct on fluid flow and heat transfer. 11 (3) (2019) 31001.